Feedback Processes in Massive Star Formation

Abstract

We propose a programme of e-MERLIN observations on a large and well-selected sample of massive young stars that spans the full range of evolutionary stages to address key questions on feedback processes. Deep continuum imaging will determine when MHD driven jets turn on and when they give way to radiatively driven disc winds and over what mass range. When the ionizing radiation first breaks out into a hyper-compact H II region we will determine the density distribution and the physical processes that have shaped it. Simultaneously, we will map the 3D magnetic field structure in a number of sources through methanol and excited OH maser polarization. Together these data will test both the physics of the feedback mechanisms and evolutionary models of massive star formation.

Name	Institution	e-mail
Melvin Hoare (Coord)	University of Leeds	mgh@ast.leeds.ac.uk
Stuart Lumsden		sll@ast.leeds.ac.uk
Rene Oudmaijer		roud@ast.leeds.ac.uk
James Urquhart		jsu@ast.leeds.ac.uk
Phil Diamond	University of Manchester	philip.diamond@manchester.ac.uk
Cormac Purcell		cormac.purcell@manchester.ac.uk
Gary Fuller		g.fuller@manchester.ac.uk
Anita Richards		a.m.s.richards@manchester.ac.uk
Wouter Vlemmings	University of Bonn	wouter@astro.uni-bonn.de
Gabriele Surcris		gsurcis@astro.uni-bonn.de
Henrik Beuther	Max-Planck-Institut für Astronomie	beuther@mpia-hd.mpg.de
Jagadeep Pandian	Max-Planck-Institut für Radioastronomie	jpandian@mpifr-bonn.mpg.de
Jim Jackson	Boston University	jackson@bu.edu
Ed Chambers		etc1@bu.edu
Jill Rathborne	CfA Harvard	jrathborne@cfa.harvard.edu
Stan Kurtz	UNAM, Mexico	s.kurtz@astrosmo.unam.mx
Luis Rodriguez		luisfr@astrosmo.unam.mx
Ed Churchwell	University of Wisconsin	ebc@astro.wisc.edu
Barbara Whitney	Space Science Institute	bwhitney@astro.wisc.edu
Claire Chandler	NRAO	cchandle@aoc.nrao.edu
Debra Shepherd		dshepher@nrao.edu
Huib Jan van Langevelde	JIVE/Sterrewacht Leiden	langevelde@jive.nl
Toby Moore	Liverpool JMU	tjtm@astro.livjm.ac.uk
Sergio Molinari	INAF - IFSI Rome	molinari@ifsi-roma.inaf.it
Antonio Chrysostomou	Joint Astronomy Centre	a.chrysostomou@jach.hawaii.edu
Mark Thompson	University of Hertfordshire	m.a.thompson@herts.ac.uk
Janet Drew		j.drew@herts.ac.uk
John Richer	University of Cambridge	jsr@mrao.cam.ac.uk
Sean Dougherty	National Research Council, Canada	sean.dougherty@nrc.ca
Jose-Maria Torrelles	IEEC, Barcelona	torrelles@ieec.fcr.es
Josep Paredes	University of Barcelona	jmparedes@ub.edu
Maite Beltran		mbeltran@am.ub.es
Riccardo Cesaroni	INAF - Osservatorio Astrofisico di Arcetri	cesa@arcetri.astro.it
Luca Moscadelli		mosca@arcetri.astro.it
Kalle Torstensson	University of Leiden	kalle@strw.leidenuniv.nl
Richard Dodson	Observatorio Astronomico Nacional	r.dodson@oan.es
Busaba Kramer	NARIT, Thailand	busaba@narit.or.th
Indra Bains	Swinburne University	ibains@astro.swin.edu.au
Simon Ellingsen	University of Tasmania	Simon.Ellingsen@utas.edu.au
Michael Burton	University of New South Wales	M.Burton@unsw.edu.au
Anuj Sarma	DePaul University	asarma@depaul.edu

Scientific Justification

High-Mass Star Formation

Massive stars play an important role in many areas of astrophysics. They impart large amounts of UV radiation, wind energy, strong shocks and enriched material into the ISM during their lifetime. The massive star population is crucial in the evolution of galaxies and when dense concentrations of such stars form, it results in starburst activity in galaxies (Leitherer 1999). Their intrinsic brightness makes them manifest in the most distant galaxies and of course they are likely to dominate the first stellar populations.

However, relatively little is known about the physics that controls the formation of stars more massive than about 8 $M_\odot$ ($10^3 L_\odot$) and hence the upper initial mass function (IMF). The fast collapse and contraction time scales and extreme conditions resulting from increased turbulence and radiation pressure, makes the theoretical treatment of their formation more challenging than for solar-type stars (e.g. Behrend & Maeder 2001; McKee & Tan 2003). Kahn (1974) pointed out that strong radiation field would reverse the infall of a spherical envelope due to radiation pressure acting on the dust. Accretion via a disc alleviates much of this problem (Yorke & Sonnhalter 2002; Krumholz et al. 2005a) as does the feedback provided by the strong bipolar outflows that puncture the cloud along the polar axis and release some of the radiation pressure (Krumholz et al. 2005b). However, here is where the enormous gaps in our knowledge appear, as to power these bipolar outflows we appeal to magneto-hydrodynamic forces as in low-mass star formation. So which force dominates, radiation or magnetic pressure, and at which stage of the evolution? If the magnetic field is so strong it powers the outflow does it also play a role in the infall and support of the cloud? We are far from an all encompassing theory, but observations can point the way.

Observationally, our understanding of the formation of low-mass stars has benefited greatly from high resolution observations of nearby examples (e.g. Pety et al. 2006). However, the rarity, and consequent increased distance, of high-mass stars, as well as their predilection to form in dense clusters with sources only a few arcseconds apart, makes their study more observationally challenging (e.g. Beuther et al. 2002). High resolution is therefore a pre-requisite in this field. With the expected sizes of accretion discs being 100-1000 AU in size and the nearest examples being at least a kpc away then 0.1 arcsecond resolution at least is required. Here radio interferometry leads the way and with ALMA to deliver the required data in the molecular material, e-MERLIN is uniquely positioned to provide the complementary picture of feedback in the ionized gas and to measure the magnetic field.

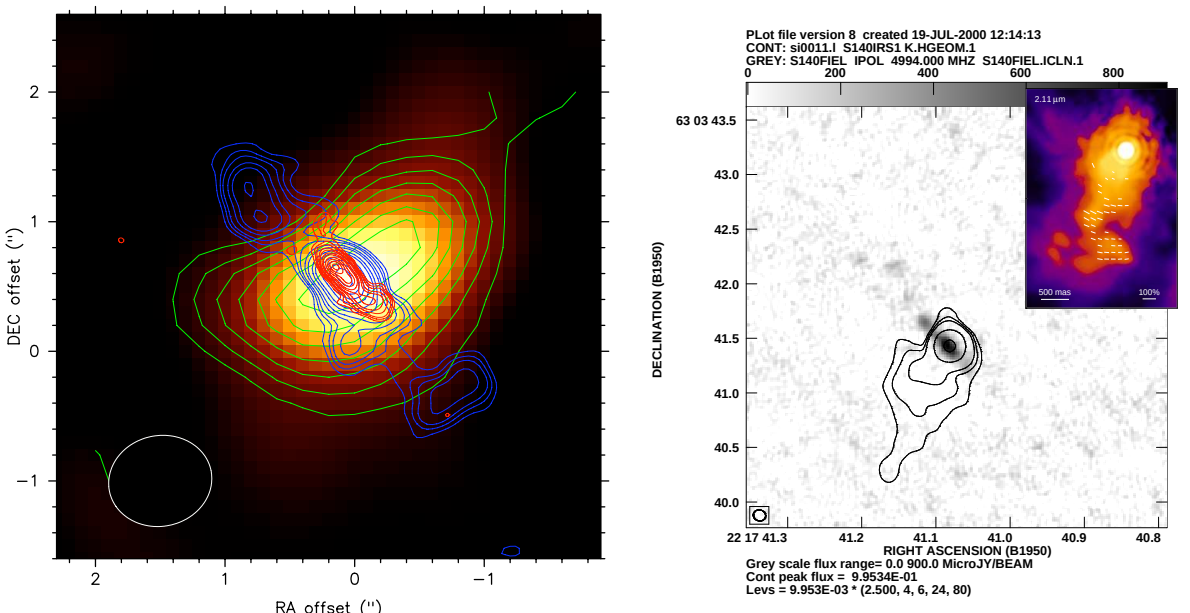

Figure 1: (a) VLA 3.6 cm (blue) and 1.3 cm (red) image of the radio jet in Cep A HW2 perpendicular to the rotating disc-like structure seen in the dust continuum (image) and CH_3CN transition (Patel et al. 2005). **(b) (Top right)** MERLIN 5 GHz image of the equatorial wind from S140 IRS 1 and monopolar 2μm reflection nebula from the blueshifted outflow lobe (Alvarez et al. 2004; and inset from Schertl et al. (2000) showing centro-symmetric polarization pattern.

Feedback

The first manifestation of fast ionized outflowing material comes in the form of ionized jets such as those from GGD27 (Martí et al. 1993) and Cep A HW2, where proper motions reveal velocities of at least 500 kms^{-1} (Martí et al. 1998; Curiel et al. 2006). The latter is perpendicular to the rotating disc-like structure seen in molecular lines and dust continuum (Figure 1a) (Torrelles et al. 2007; although see Comito et al. 2007 and unexplained features in the MERLIN 1.6 GHz map by Hoare & Garrington 1995). Other possible radio jets from massive YSOs are GL 2591 (Trinidad et al. 2003), IRAS 20126+4104 (Hofner et al. 2007) and IRAS 18089-1732 (Beuther & Walsh 2008). The typical mass-loss rates in these jets are about $10^{-}6M_{\odot}yr^{-1}$ (Marti et al. 1999). These radio jets are similar to the those that have been resolved in low-mass YSOs in several cases (Anglada 1996) and therefore assumed to be a scaled-up version of these MHD driven and collimated flows. These are likely to play important roles in the removal of angular momentum from the accreting system (Coffey et al. 2007); driving the much larger scale bipolar molecular flows (Downes & Cabrit 2007), and entraining large volumes of the surroundings in motion (Arce et al. 2008) thereby adding to the turbulence with potential knock on effects for subsequent star formation (Mac Low 2008).

Further strong feedback occurs for the more luminous sources when ionization of the surrounding material begins. The expanding ionization front of the nascent H II region moves faster in low density directions, most likely to be the polar lobes. In this scenario, one would expect the youngest, most compact H II regions to be bipolar. Within the class of so-called hyper-compact H II regions (HCHII, see Kurtz 2005) there are examples of bipolar objects. These also tend to display broad recombination lines ($\gtrsim$40 km s^{-1}) (Jaffe & Martin-Pintado 1999; Sewilo et al 2004). Of particular interest is NGC 7538 IRS (Hoare et al. 2007) which has bipolar lobes with velocity widths in excess of 100 km s^{-1} (Gaume et al. 1995) and are getting significantly fainter on a timescale of 10 years (Franco-Hernández et al. 2004). The short lifetime would be consistent with the rarity of objects in a crucial transition stage.

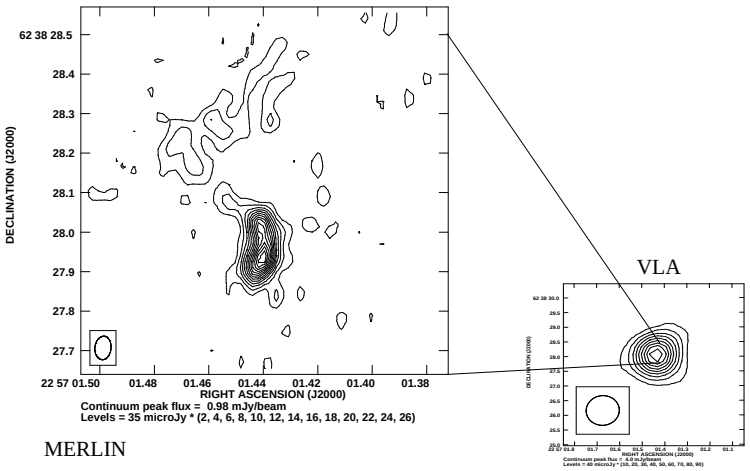

Figure 2: MERLIN 5 GHz image of the hyper-compact H II region G110.209+2.630. Deeper, higher fidelity imaging by e-MERLIN will enable us to tell if this, and others are bipolar objects in a transition phase. From Kurtz et al. in prep. with unresolved 8 GHz VLA image from Kurtz et al. (1994).

Other hyper-compact H II region exhibit a variety of morphologies which tell us about the density distribution immediately after the turn on of the ionizing radiation field. Some exhibit the cometary morphology that is common in more evolved UCHII regions (Hoare et al. 2007) and is likely due to being located in a strong density gradient (Arthur & Hoare 2006). Others have a shell morphology indicating a location at the centre of a density concentration rather than the off-centre cometary objects. Statistics on the different types of morphology could tell us whether massive stars are predominately forming (presumably via spontaneous collapse) at the centres of dense cores, or more often off-centre, perhaps due to the triggering of collapse by the passage of an external shock.

Some of the less luminous and less embedded massive young sources exhibit the opposite radio morphology to the radio jets described above. MERLIN observations have shown that S106IR (Hoare et al. 1994) and S140 IRS 1 (Hoare 2006; see also Drew et al. 1993) (Figure 1b) are elongated perpendicular to the molecular bipolar outflow axis and are instead aligned with the inferred plane of

the accretion disk. The estimated mass-loss rates in these disc winds are also of order $10^{-}6 M_{\odot} yr^{-1}$ (e.g. Drew et al. 1993). These 'equatorial winds' have been interpreted as radiatively driven disc winds (Drew et al. 1998) where the pressure due to the strong radiation field blows the disc surface sideways out of the system with velocities of several hundred km s^{-1} similar to the widths of the H I emission lines in the IR (Sim et al. 2005). This picture is in the same spirit as the possible evolutionary scenario in which MHD driven jets early on give way to less-collimated radiation pressure dominated flows at later stages proposed by Beuther & Shepherd (2005). As the stars emerge from their natal cloud as Herbig Be stars many still show evidence for strong disc winds. MWC 297, was partially resolved with MERLIN showing a quadrapolar morphology (Drew et al. 1997), whilst AMBER VLTI observations of the Brγ line are interpreted as a disc wind (Malbet et al. 2007). It is not known whether this final stage of the feedback process of disc erosion by the ionized wind finally results in the shutting off of accretion or prevents planetary formation around massive stars.

Up to this point current facilities have only been able to skim the surface by mapping just a few of the nearest and brightest examples and are nowhere near a big enough sample to begin to tell us which mechanisms dominate, over which mass range, and which stage of evolution. e-MERLIN can map a statistically significant sample to make real progress in understanding the physics of feedback.

Magnetic fields during massive star formation

Simultaneously with the continuum mapping of jets and disc winds, e-MERLIN can deliver on another key aspect of star formation physics: the magnetic field. In low-mass star formation, magnetic fields are thought to regulate the accretion onto the proto-star from a proto-stellar disk, and to collimate the outflow (e.g. Konigl & Pudritz, 2000). Their role in regulating the initial collapse within star forming clouds, likely through ambipolar diffusion, is however still unclear (e.g. McKee & Ostriker 2007), although linearly polarized dust continuum emission has recently shown the ambipolar diffusion predicted pinched hour-glass shaped magnetic field morphology towards a low-mass system (Girart et al. 2006). Massive stars are fully radiative and hence are typically not expected to have significant magnetic fields, although there are exceptions (Donati et al. 2006). However, bipolar molecular outflows are known to be as ubiquitous during high- as during low-mass star-formation, and if the launching mechanisms of these outflows are of similar nature, strong magnetic fields must also be present in dense massive cores (e.g., Arce et al. 2007). Maser polarization observations play an especially important role, as these are the only observations that can reveal both the 3-dimensional magnetic field morphology and strength close to MYSOs and thus directly probe the relation between the field and the continuum morphology.

Maser polarization measurements

Masers probe the magnetic field in the intermediate to high density regions of massive star forming regions ($n_{H_2} \gtrsim 10^5 cm^{-3}$). Observations of the Zeeman effect in the dense H_2O maser regions reveal dynamically important magnetic fields (e.g. Sarma et al. 2008; Vlemmings et al. 2006a) while the linear polarization measurements reveal a complex but often ordered magnetic field morphology. Aside from H_2O masers, tracing high density and typically shocked regions, the (weaker) magnetic field in the less dense surrounding regions is probed by polarimetric OH maser observations (e.g. Bartkiewicz et al. 2005) and detailed modeling of MERLIN observations has been used to describe the rotating disc-bipolar outflow system of W75N (Hutawarakorn et al. 2002; Gray et al. 2003). However, both internal and external Faraday rotation make a direct interpretation of the 1.6 GHz OH maser polarization difficult (Fish & Reid 2006). This problem is alleviated by observing maser transitions at higher frequencies, such as the excited state OH masers at 6 GHz and the methanol masers at 6.7 GHz.

The 6.7 GHz methanol masers are likely pumped by a combination of collisions and emission from nearby, warm ($T > 150$ K) dust, but themselves arise in cool ($T < 50$ K) dense gas ($n_{H_2} > 10^6$ cm^{-3}) with high methanol abundance (e.g. Sobolev et al. 1997; Cragg et al. 2005). Like H_2O, methanol is a non-paramagnetic molecule, and thus any polarization is small with interferometric 6.7 GHz maser measurements finding linear polarizations from 2-10% (Ellingsen et al. 2002; Vlemmings et al. 2006b; Dodson 2008). From the direction of the linear polarization vectors, we obtain the direction of the

magnetic field in the plane of the sky (Figure 3). By further comparing the polarization fraction with sophisticated maser models, similar to those for H_2O masers described in Vlemmings et al. (2006a), we will be able to place stringent constrains on the angle between the magnetic field and the line of sight. Consequently we will be able to describe the *full 3-D morphology of the magnetic field*. The first circular polarization measurements have recently be made with the Effelsberg telescope showing Zeeman splitting (Vlemmings 2008). These observations revealed strong, dynamically important, magnetic fields for 18 out of 24 observed massive star forming regions, with a deprojected average magnetic field strength of $|B| = 23$ mG (Fig. 3, right).

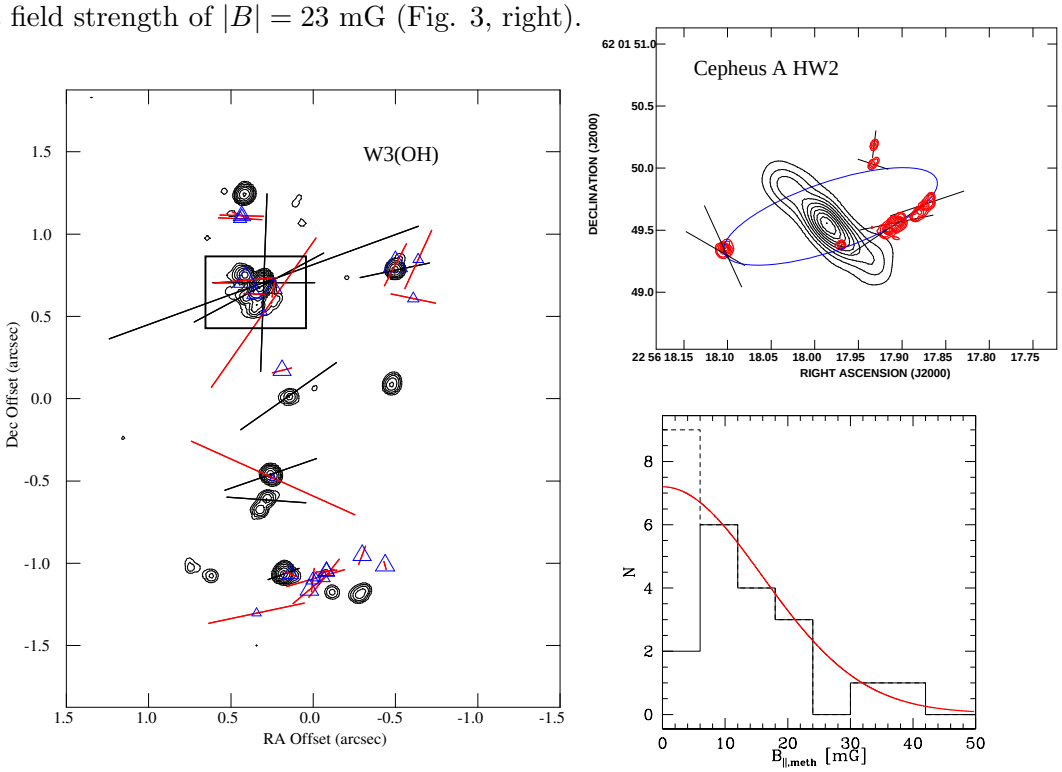

Figure 3: left MERLIN linear polarization map of 6.7 GHz methanol masers in W3 (OH) with vectors (black) indicating the magnetic field is parallel to the elongated maser structure (Vlemmings et al. 2006b) (1.6 GHz OH maser polarization in red, Wright et al. 2004). The 'broadline' region (boxed) is likely a very young object within or behind an UCHII region. **(top right)** Same for Cepheus A HW2 with vectors following the elliptical maser distribution perpendicular to the VLA jet (contours). **(bottom right)** Distribution of line-of-sight magnetic field strength including non-detections due to field orientation (dashed) and expected distribution if homogeneous (red).

Evolutionary Sequence

As discussed above there appear to be different forms of feedback, jets, hyper-compact H II regions and ionized disc winds, occurring at different evolutionary stages and luminosity (mass) ranges and the importance of the magnetic field will also change. To begin to put this together in a coherent picture we need an evolutionary sequence for massive star formation. All stars are born deeply embedded and emerge over time as the surrounding material is either accreted or dispersed. In broad terms, therefore, the peak of the spectral energy distribution (SED) must shift from longer (submm) to shorter (infrared) wavelengths. An evolutionary sequence based on SED shape has been successfully used in low-mass star formation for decades (Lada & Wilking 1984, André et al. 1993, Shirley et al. 2002). An analogous sequence has been sketched out for high-mass star formation (e.g. Evans et al. 2002, Kurtz et al. 2000), but as yet remains mostly that - a sketch.

Of particular interest recently has been the discovery of clouds that are opaque at 8μm, so called IR dark clouds (IRDCs), which are dense, cold and massive enough to be the precursors of massive stars (Rathborne et al. 2006). Quite a number of them already show signs of star formation as embedded point sources are seen at 24μm and 70μm by Spitzer (see Figure 4). We refer to these as 'active IRDC sources' and they currently represent earliest stage of the newly forming massive stars. As the surrounding molecular gas is warmed by the growing star, ice mantles are sublimated back into the

gas phase. In this 'hot molecular core' phase (e.g. Viti et al. 2004) some molecules such as water and methanol become highly visible due to masing activity. Hot core (Rathborne et al. 2007) and water and methanol maser activity (Wang et al 2006; Ellingsen 2006) have been seen in some IRDC sources, as well as later stages. Another manifestation of activity are the bipolar outflows seen emerging from IRDCs at 4.5μm due to shocked molecular hydrogen (Cyganowski et al. 2007).

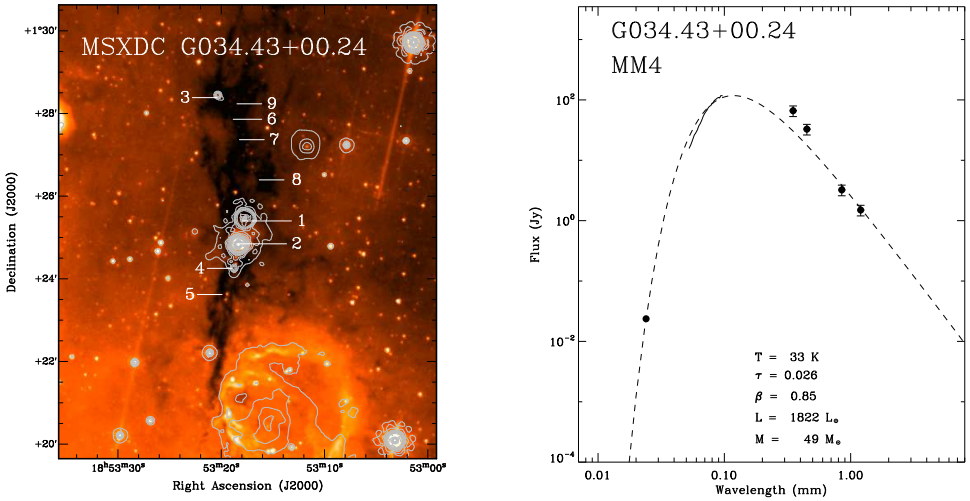

Figure 4: (a) Spitzer 8μm image of G034.43+00.24 showing the filamentary dark cloud and the active IRDC sources MM1, the UCHII region 2 and the fainter IRDC source MM4 just to the S. **(b)** SED of MM4 from Spitzer 24μm, MIPS SED mode spectrum and submm/mm photometry. From Rathborne et al. in prep.

Once the envelope gets significantly dispersed by the outflows the object becomes visible first in the mid-IR and then near-IR. These are manifest as the mid-IR bright massive YSOs. These stars are luminous, probably core burning hydrogen, and yet do not ionize the surrounding ISM to form a UCHII region. The answer may be due to their swollen size and low T_{eff} caused by ongoing accretion at high rates as shown recently by Hosokawa & Omukai (2008). When accretion does shut off the star can rapidly settle onto the main sequence and begin to ionize the hyper- or ultra-compact H II region stage. As feedback clears away most of the obscuring cloud the lower mass end of the OB stars still retain the signatures of youth such as IR excess and strong emission lines as Herbig Be stars.

Overall, there is a trend from deeply embedded to optically visible but there is little underlying theoretical basis for a scheme and much overlap between the observationally defined object types. So here we will adopt the basic premise of colour evolution and address the fact there is expected to be considerable intrinsic scatter in any SED scheme. This is due to the asymmetry in the circumstellar density distribution caused by the flattening envelopes and outflow cavities. Therefore viewing angle as well as age signficantly affects IR colours (Yorke & Bodenheimer 1999; Whitney et al. 2003), as does clumpiness (Indebetouw et al. 2006). Here again large samples are the key to overcoming this intrinsic natural scatter.

Sample selection from Galactic Plane Surveys

The burgeoning of multi-wavelength Galactic Plane surveys allows us for the first time to select large samples free from many of the previous biases. We will select from the distribution in L_{bol} versus IR colour diagrams which represent mass and evolutionary stage respectively. For the earliest phases, the MSX and GLIMPSE surveys have delivered the IRDC sample (Simon et al 2006), whilst MIPSGAL is now revealing the active sources. We will select a sample of these sources that satisfy the criteria of luminosity >2000 $L_{\odot}$ (equivalent to B3V and earlier), invisible in Spitzer 8μm images, 70μm/24μm flux ratio $\gtrsim$50 (Figure 5a) and distance <7 kpc. Luminosities are derived from kinematic distances from the GRS survey of ^{1}3CO 1-0 and far-IR fluxes from fits to the SED (Figure 4, Rathborne et al. in prep). The work of measuring the 70μm fluxes is still ongoing (the MIPSGAL team have not yet released a catalogue), and 11 of these IRDC sources are currently included in Table 1 with the aim 30 in total. Many of the active IRDC sources are also methanol maser sources (Ellingsen 2006). The Methanol Multi-Beam (MMB) (Green et al. 2007) and deeper Arecibo (Pandian et al. 2007)

surveys, allow the systematic selection of methanol masers for magnetic field studies in addition to SED selection for the evolutionary stage. Others sources are known methanol masers from previous work and 11 such objects known not to be mid-IR bright are currently listed in Table 1. They will *only* be included in the final 30 IRDC sample if they satisfy the selection criteria set out above which requires the analysis of archive Spitzer data which is ongoing.

For the mid-IR bright MYSO sample we will select from the Red MSX Source (RMS) survey (Hoare et al. 2005). The selected sample satisfy the same distance and luminosity cut as above, have 21μm/8μm flux ratio >2 (Figure 5b) and are radio quiet IR point sources, i.e. they have not been detected at the mJy level and so are not yet at the UCHII region phase. Their 70μm/24μm flux ratios go up to about 100 where they join seamlessly with the IRDC sources so there is no gap in our selection (see Figure 5a). For most of our MYSO targets we have near-IR spectra showing they are likely to be still accreting (CO bandhead emission, e.g. Chandler et al. 1995) and driving ionized winds (weak Brγ emission, Bunn et al. 1995). We will target 60 MYSOs (Table 2) as this is the phase where the transition from magnetically driven jets to radiatively driven disc winds is thought to take place and a sufficient sample of each is required to understand the trends with mass and age. Many of the MYSOs are also methanol maser sources and will have their magnetic fields studied at the same time. Only the strongest masers can be studied fully with circular polarization and to ensure against biasing our sample by only including strong maser sources we again need at least as many weak or non-masing MYSOs. The large sample size also alleviates this.

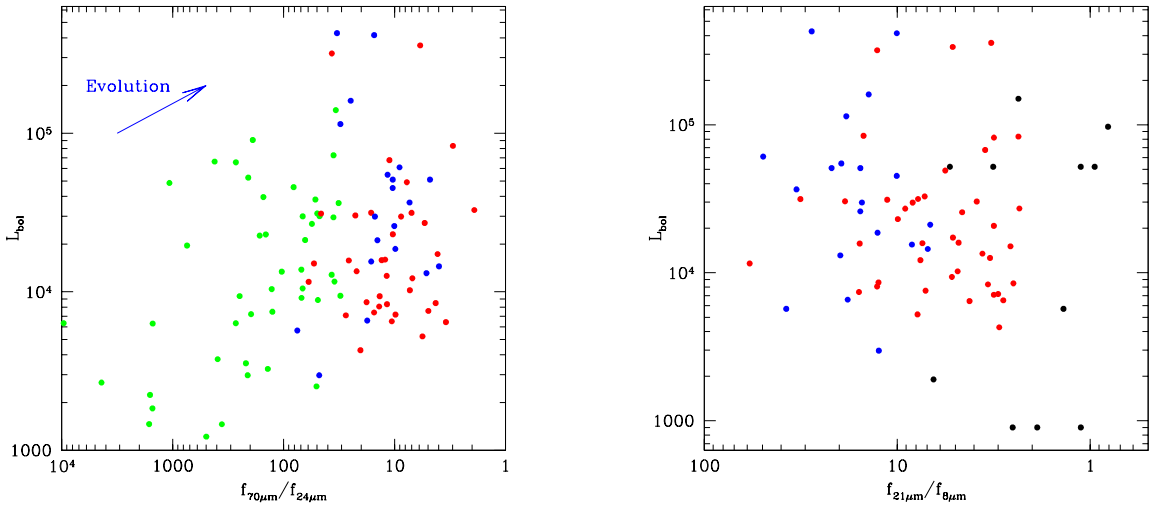

Figure 5: (a) L_{bol} versus far-IR colour diagram for active IRDC sources (green), candidate HCHII regions (blue) and MYSOs (red). The IRDC sources are from 24μm sources seen in IRDCs (mostly the redder sources) and methanol masers sources from MMB for illustrative purposes. This is not the final sample which will be selected according to the criteria set out in the text. **(b)** L_{bol} versus mid-IR colour diagram for candidate HCHII regions (blue), MYSOs (red) and Herbig Be stars (black). The latter are from the catalogue of The et al. (1994) and are illustrative only. The final sample will be selected as described in the text.

Candidate hyper-compact H II regions come from the CORNISH survey (Purcell et al. 2008) and the RMS survey. 30 UCHII regions are unresolved in the VLA B configuration data and satisfy the same colour cuts as the MYSOs (Figure 5a & b) (Table 3). The distance cut has been relaxed to 9 kpc to ensure a large enough sample for these rarer objects. Finally we will target 30 Herbig Be stars selected from the IPHAS survey (Drew et al. 2005; Witham et al. 2008) cross-matched with GLIMPSE/MIPSGAL/MSX and associated with star forming regions. The same luminosity and distance (from spectral type and photo-metric parallax) and cuts will be applied. Some Herbig Be stars (e.g. V645 Cyg) overlap with the RMS MYSO sample whilst others are bluer than the 21μm/8μm $>$ 2 cut (Figure 5b). The identification of Herbig Be stars from IPHAS is ongoing, but the selection work for these and the other stages will be completed well ahead of the start of the Legacy Programme observations.

Taking the sample of 150 sources across the L_{bol} versus IR colour selection diagrams as a whole we can divide them into 3 luminosity bins and 5 colour bins and still leave 10 sources in each bin which

should be sufficient to overcome the scatter due to viewing angle. Simulations using the Whitney et al. (2003) radiative transfer models will be carried out to investigate the effect of different viewing angles and quantify the remaining uncertainty after averaging over the sample.

The role of e-MERLIN

Continuum measurements The combination of sensitivity and resolution that e-MERLIN provides means it is the only facility capable of resolving the radio emission from the large sample of objects required to make progress. To obtain the sample size we necessarily have to go to 7 kpc away to probe sufficient volume. The VLA is barely resolving the closest ($\sim$ 1 kpc) and brightest examples at present and will not be able to resolve the more distant examples. Going to higher frequencies does not help much because jet and wind sources get smaller with increasing frequency ($\theta \propto \nu^{-0.6}$, e.g. Gibb & Hoare 2007; Wright & Barlow 1975). For wind sources there is no substitute for baseline length, and the 300 AU resolution of e-MERLIN at 6GHz at 7 kpc is sufficient to resolve the type of structures seen in the nearby examples. We will use this resolution and depth to:

- Determine at which evolutionary stage and luminosity the MHD jets turn on. Are the earliest active IRDC sources already driving jets or in a pure infall phase?
- Find out how jet parameters (strength, collimation) vary as a function of luminosity and evolutionary stage? These will be compared to disc properties (ALMA) and used to test jet models.
- Determine at what evolutionary stage the switch from magnetically driven jets to radiatively driven disc winds occurs for each mass range.
- Measure how the disc wind strength varies with luminosity and test radiative driving models ($\dot{M} \propto L^{1.5}$).
- Search for rare transition phase objects where the ionization has recently switched on. What is the distribution of bipolar, shell or cometary morphologies at the earliest stages and what are the implications for massive star formation models?

Magnetic field observations Only the resolution of e-MERLIN allows us to probe the magnetic field strength and geometry on 100-1000 AU scales where the influence of the disc and jet launching are occurring (e.g. Harvey-Smith & Cohen 200). The specific goals of the e-MERLIN maser observations are:

- Constrain the 3-dimensional magnetic field morphology from methanol and OH maser linear polarization observations and consequently, for a subset of sources, determine the total magnetic field strength through Zeeman observations. The shape and strength of the magnetic field is a crucial input to MHD modeling of massive star formation.
- Directly relate the continuum morphology, such as jets and outflows, to the magnetic field geometry as illustrated in Fig. 3.
- Relate the continuum morphology, to the maser spatial and velocity distribution. This will for example provide important constraints on the origin of methanol masers, which have been argued to occur on discs, shocks or outflows.
- As linear polarization depends on the maser saturation level, fractional linear polarization measurements will put limits on maser saturation levels and intrinsic maser properties.

The combination of continuum properties and magnetic field constraints over such a broad and well-selected sample will provide a stern test for massive star formation models as they develop. We will compare the orientation of the major axes of the continuum structures with outflow indicators such as CO outflows (many already studied and ongoing) and bipolar IR reflection nebulae or shocked emission. This will classify them as jets or disc winds. Each type will then be placed in an evolutionary context and used to test different models. For the early stages these will be ones with increasing accretion rate (e.g. McKee & Tan 2003; Krumholz et al. 1995) where some fraction is removed as an ionized wind, whilst for the later stages we will be testing disc destruction by radiatively driven wind ablation (e.g. Drew et al. 1998). The results will set the physics of feedback in massive star formation on a firm basis for the first time.

References

Alvarez C. et al 2004, A&A 427, 505
Andre, P.; et al., 1993, ApJ, 406, 122
Anglada G., 1996, in ASP Conf. Ser. p 3
Arce, H. G. et al, 2007, in PPV p 245
Arthur S., Hoare M., 2006, ApJS, 165, 283
Bartkiewicz A et al. 2005, MNRAS 361, 623
Behrend R., Maeder A., 2001, A&A, 373, 190
Beltran, M., et al. 2001 AJ, 121, 1556
Beuther, H. et al. 2002, A&A, 387, 931
Beuther, H.; Walsh, A. J., 2008, ApJ, 673, L55
Beuther, H.; Shepherd, D., 2005, in ASSL, 325, p105
Bunn J. et al, 1995, MN, 272, 346
Chandler C. et al, 1995, ApJ, 446, 793
Coffey, D, et al. 2007, ApJ, 663, 350
Comito, C., et al. 2007, A&A, 469, 207
Cragg D et al. 2005, MNRAS 360, 53
Curiel S., et al, 2006, ApJ 638, 878
Curran & Chrysostomou 2007 MNRAS, 382, 699
Cyganowski, C, 2007, AAS, 211, 8904
de Wit, W. J. et al. 2007, ApJ, 671, L169
Dodson 2008, A&A 480, 767
Drew, J. E., et al. 2005, MNRAS, 362, 753
Drew J.E., et al, 1998, MNRAS, 296, L6
Drew J.E., et al, 1997, MNRAS, 286, 538
Donati, J. F., et al., 2006, MNRAS, 365, L6
Downes, T. P.; Cabrit, S., 2007, A&A, 471, 873
Ellingsen S et al. 2002, IAU Symp 206 15
Ellingsen, S. P., 2006, ApJ, 638, 241
Evans, N. J.; et al. 2002, ASP Conf Proc, 267.
Fish V. & Reid M. 2006, ApJS 164, 99
Franco-Hernandez R.et al. 2004, ApJ 604, L105
Gaume R. A., et al. 1995, ApJ, 438, 776
Gibb, A. G., Hoare, M. G., 2007, MNRAS, 380, 246
Girart et al. 2006, Science 313, 812
Gray M. et al. 2003, MNRAS 343, 1067
Green J., et al. 2007, IAU Symp, 242, 218
Harvey-Smith L & Cohen J. 2006, MNRAS 371, 1550
Hoare M.G., Garrington S.T., 1995, ApJ, 449, 874
Hoare M. G., et al., 1994 , ApJ, 421, L51
Hoare M. G. et al, 2005, In IAU Symp. 227, p 370
Hoare M.G. 2006 ApJ 649, 856
Hoare M. et al, 2007, in PPV p 181
Hofner P., et al. 2007, A&A, 465, 197
Hosokawa, T., Omukai, K., 2008, in ASP Conf,387, p.255
Hutawarakorn et al. 2002, MNRAS 330, 349
Indebetouw, R. et al. 2006, ApJ, 636, 362
Jaffe D. and Martin-Pintado J. 1999, ApJ, 520, 162
Kahn,F. D. 1974, A&A,, 37, 149
Konigl A & Pudritz,R. 2000 in PP IV
Krumholz, M. R., et al., 2005a, in IAU Symp, 227, 231
Krumholz, M. R., et al., 2005b, ApJ, 618, L33
Kurtz, S., 2005, in IAU Symp, 227, CUP, p 111
Kurtz, S., et al., 2000, in PP IV, 299.
Kurtz et al., 1994, ApJS, 91, 659
Lada, C. J.; Wilking, B. A., 1984, ApJ, 287, 610
Leitherer, C., 1999, IAU Symp. 186, 243
Mac Low, M. M, 2008, ASP Conf. Ser. 387 p 148
Malbet, F., et al. 2007, A&A, 464, 43
Marti, J., et al. 1999, A&A, 345, L5
Marti, J., et al. 1998, ApJ 502, 337
Marti, J., et al. 1993, ApJ, 416, 208
McKee, C. F., Tan, J. C., 2003, ApJ, 585, 850
McKee C. F., & Ostriker, E. 2007 ARAA 45, 565
Pandian, J., et al., 2007, ApJ, 656, 255
Patel N. et al, 2005, Nature 437, 109
Pety J., et al. 2006, A&A, 458, 841
Purcell, C. et al. 2008, ASPC, 387, 389
Rathborne, J. M.; et al. 2006, ApJ, 641, 389
Rathborne, J. M.; et al. 2007, ApJ, 662, 1082
Reynolds, S. P., 1986, ApJ, 304, 713
Sarma A. et al. 2008 ApJ 674, 295
Schertl, D., et al. 2000, A&A, 361, L29
Sewilo, M. et al. 2004, ApJ, 605, 285
Shirley Y. L., et al. 2002, AJ, 575, 337
Sim S. et al, 2005, MN 363, 615
Simon, R. et al. 2006, ApJ, 639, 227
Sobolev A et al. 1997, A&A 324
The, P. S., et al., 1994, A&AS, 104, 315
Torrelles, J. M., et al. 2007, ApJ, 666, L37
Trinidad M. A., 2003, ApJ, 589, 386
van der Walt 2005, MNRAS 360 153
Viti, S., et al. 2004, MNRAS, 354, 1141
Vlemmings W. et al. 2006a, A&A 448, 597
Vlemmings et al. 2006b, MNRAS 371, L26
Vlemmings 2008, A&A 484, 773
Wang, Y., 2006, ApJ, 651, L125
Whitney B. et al, 2003, ApJ 591, 1049
Witham, A. R., 2008, MNRAS, 384, 1277
Wright et al. 2004, MNRAS 350, 1272
Wright A.E., Barlow M.J., 1975, MNRAS, 170, 41
Yorke, H. W., Sonnhalter, C. 2002, ApJ, 569, 846
Yorke H. W., Bodenheimer P., 1999, ApJ, 525, 330

Related Datasets

Obviously this programme relates to the multi-wavelength Galactic Plane surveys that are the springboard for the selection of large, well-defined samples that enable it. These are the IPHAS, 2MASS/UKIDSS GPS, GLIMPSE, MIPSGAL, MSX, GRS, MMB, Arecibo, and CORNISH surveys. Upcoming surveys will also feature strongly in the exploitation and interpretation of the results from this survey. These include the JCMT SCUBA2 survey and Hi-GAL survey with HERSCHEL that will complete the SEDs in the far-IR/sub-mm regime which especially important for the cold, early stages. They will also set the IRDC sources in a wider context that does not rely on a particular geometry to produce the dark cloud absorption.

The main other related e-MERLIN Legacy programme is the one on low-mass YSO jets. This is highly complementary as it will provide close-up tests of jet models through the multi-epoch studies of objects 10 times closer than those here. Lessons learned from that programme can then be tested on the higher luminosity jets found in this programme to look for systematic differences with mass. This will be a stern test of the 'scaled-up version of low-mass star formation' put forward for high-mass star formation. To ensure continuity across these programmes Rodriguez and Richer are members of this team and Hoare is a member of the low-mass team.

Another prime motivation for a large coordinated programme such as this is that it will provide a very strong case for the ALMA time required to provide the molecular line and dust continuum data at the commensurate resolution (see next section).

A number of the maser sources in our sample are the target of high resolution submm dust polarization observations with the SMA, while several of the sources accessible from the Southern hemisphere will be targeted by ALMA in the future. Additionally, several have been targeted with the JCMT, for example in the SCUBA polarization observations by Curran & Chrysostomou (2007). Future JCMT instruments will further probe dust polarization as well as thermal line Zeeman splitting at large scales. The 3-dimensional magnetic field models derived from the data of this e-MERLIN legacy project can thus be directly compared with the magnetic field morphology and strength observed in the lower density envelopes around the MYSO.

Technical Justification

We propose to image the 5-7 GHz continuum in a total sample of 150 sources across the full range of evolutionary stages: 30 IRDCs, 60 MYSOs, 30 potential HCHIIs and 30 Herbig Be stars. The estimated mass-loss rates in the ionized jets and disc winds seen in the nearby examples of MYSOs are about 10^{-6}M$_\odot$yr^{-1}. Estimates of the accretion rates in these systems are very difficult to obtain, but in the context of current theory (e.g. see McKee & Tan 2003 Figure 2) it is reasonable to assume that these objects are reasonably far along in their formation (few 10^4 years) and accreting at a rate of order 10^{-4}M$_\odot$yr^{-1}. This would imply the ratio of ionized mass-loss rates to accretion rate is about 1% which is conservative in jet and disc wind models where the total outflow/inflow ratio is often quoted as about 10% (Königl & Pudritz 2000). Here we want to probe the first few thousand years when the source is still likely to be in the IRDC stage and the accretion rate is more like 10^{-5}M$_\odot$yr^{-1} in the McKee & Tan scenario. This means we have to probe jets with mass-loss rates of 10^{-7}M$_\odot$yr^{-1}.

We follow Beltran et al. (2001) who use the radio jet theory of Reynolds (1986) and find that if we assume a typical spectral index of 0.6, jet openning angle of 30^o, wind temperature of 10^4K, jet speed of 500 km s^{-1}, then the flux at 6 GHz is given by $S_{nu} = 9\dot{M}_{-6}^{4/3} d^{-2}$ mJy where $\dot{M}_{-6}$ is the mass-loss rate in 10^{-6}M$_\odot$yr^{-1} and d is in kpc. Hence, even for our most distant (7 kpc), youngest sources we expect 9μJy. Most of the sources will be much brighter and resolved. The nearest jets and winds are about 0.5″ FWHM along the major axis and so will be about two beams across at 7 kpc. The minor axis is usually unresolved so far.

The eMERLIN correlator provides a raw bandpass of 2048 MHz divided into sixteen 128 MHz sub-bands. Two sub bands are adequate to cover the methanol and OH maser lines, while the remaining fourteen sub-bands will be allocated to observe the continuum, delivering a bandwidth of 1792 GHz. To minimize time-smearing and enable subtraction of confusing sources throughout almost the entire primary beam, we will use a 1-second cycle time. Observations will be conducted in full polarisation mode (Stokes I, Q, U and V) and the maximum data rate of 25 Mb/s then limits the number of channels per sub-band to 256. In this configuration bandwidth smearing will be minimised across the full 5 arcmin field of view imposed by including the Lovell antenna in the array. The 2048 MHz wide correlator band will be centered on 6 GHz, encompassing the 6.668618 methanol and 6.035092.GHz OH maser lines. The efficiency of the Lovell antenna falls is still an acceptable $\eta = 0.67$ at 7 GHz, and most of our sources have spectral indices of about $\nu^{0.6}$, more than compensating for the drop in sensitivity.

We propose to image down to a continuum root-mean-square (RMS) noise level of $\sim$3μJy/beam . Including the Lovell antenna the quoted sensitivity at 5 GHz for 12 hours on-source is approximately 2μJy/beam. A RMS noise of $\sim$3μJy/beam is reached after 5-hours on-source. At the high frequency end of the bandpass (6.7 GHz) the efficiency of the Lovell antenna drops by 13 percent, however, we expect the spectral index of our sources to rise as $\nu^{0.6}$, more than compensating for the decrease in sensitivity. This noise levels allows to achieve our aims.

We will alternate between two sources during each 12 hour track. At frequencies of 5-7 GHz, and for the longest eMERLIN baseline, phase decorrelation time ranges from $5-40$ minutes, depending on the atmospheric conditions. To track these changes we will bracket each source scan by observations of a nearby phase calibrator. Where possible, we will select one of the two science sources to contain a methanol maser, providing an additional method of refining the calibration via self-calibration. Hence, overall we require 900 hours to complete this programme.

Maser line observations

To observe the methanol and excited OH maser lines simultaneously with the continuum, we will include a number of spectral zooms covering the 6668.618 GHz methanol masers and the 6035.092 GHz excited OH maser line. Taking into account the data rate limit of 25Mb/s, the methanol line will be observed with 4096 spectral channels over a 2 MHz bandwidth for a spectral resolution of 0.02 km s^{-1}and a total velocity width of $\sim$ 83 km s^{-1}. The OH line is covered with a 2 MHz band with 1024 channels, also giving a total width of $\sim$ 83 km s^{-1}and a spectral resolution of 0.1 km s^{-1}. The total bandwidth is sufficient to detect the maser emission even for those sources where no accurate maser velocity is known. We will observe in full polarization mode to construct all 4 stokes parameters and will use

a 1 sec integration time. The expected 3σ channel sensitivity for 5 hours on source will be 22 and 11 mJy/beam for the methanol and OH masers respectively.

As a large number of the IRDCs, MYSOs as well as ultra-compact HII regions will have methanol and/or OH masers, over half of the sources in our sample will have detectable maser emission. To determine the magnetic field morphology and its relation to jets and outflows, we need to be able to detect linear polarization. With the e-MERLIN sensitivity we will be able to detect linear polarization on maser features as weak as ~ 0.5 Jy/beam and ~ 0.1 Jy/beam for the OH masers as the narrow channel width will allow us to smooth the spectra to the optimal width for polarization detection. We can estimate, following the analysis by van der Walt (2005), that at least $> 75\%$ of the methanol masers will be sufficiently strong. Thus, the magnetic field will be imaged for at least 50 sources in our sample. The significantly weaker circular polarization level ($\sim 0.2\%$) can be detected for methanol maser sources with fluxes > 15 Jy/beam and for somewhat weaker OH maser sources. For ~ 20 of these sources the masers will thus be strong enough to also directly map the magnetic field strength.

Declination spread and the addition of the Chilboloton Dish

Many of our proposed targets are between declinations -10^o and +20^o, which is not ideal for the current e-MERLIN, but derives from two important scientific reasons. First, the sample selection arises mainly from Galactic Plane surveys in the GLIMPSE region. Secondly, equatorial targets will allow follow-up by the main high resolution facilities needed to complete the picture of high mass star formation. Namely, ALMA, to probe the distribution and dynamics of the infall and outflow on comparable spatial resolutions to that provided by e-MERLIN, particularly for the early stages. For the later, stages VLTI interferometry with MIDI is vital to probe the inner dust envelope (de Wit et al. 2007) and with AMBER to yield spatially resolved kinematics of winds (Malbet et al. 2007).

Given the importance of this aspect two institutions on this proposal team, Leeds and Herts., are part of the consortium that has raised £500k towards the inclusion of the Chilbolton dish in the e-MERLIN array. Its southerly location would mean much better beam shape for equatorial sources and allow a good synergy with the high resolution facilities in Chile. This programme is not dependent on the inclusion of Chilbolton for success, but it would aid this and other Legacy programmes.

Requirements for pipeline processing/data archiving

It is anticipated that the bulk of the continuum data-reduction will be done at JBCA using AIPS. Considerable experience exists within the consortium on the development of data reduction pipelines utilising AIPS, for example the CORNISH pipeline. We will leverage this experience to fast-track the development of an e-MERLIN continuum pipeline. The large bandwidth of the new correlator will require new calibration and imaging strategies, which are currently being developed at JBCA.

Initial data products will be inspected by an experienced MERLIN user before being released to the consortium for verification. Final data products will be released to the community via a web-based data server. These will consist of calibrated *uv*-data, pipeline-reduced images and catalogues of sources, all in VO-compliant formats.

For reduction of the line data (including polarization), continuum calibration solutions will need to be transferred to the line data. Transferring calibration solutions in this manner is needed by a variety of other spectral line experiments (such as evolved star observations) and the consortium will be able to contribute manpower to the common development of the required pipeline processes. Further processing of the line polarization data, such as imaging and polarization analysis will be done at a number of the institutes involved in the consortium.

Management and Resource plan

Management structure The project will be managed by the leaders of the two sub-tasks, Hoare and Vlemmings. They will be assisted in the data gathering and initial reduction by a team consisting of Purcell (PDRA who developed the CORNISH data reduction and imaging pipeline); Richards (support astronomer with many years experience of MERLIN spectral line work), Fuller (academic with significant interferometry experience) and Diamond (academic with decades of spectral-line interferometry experience). This group is part of the e-MERLIN commissioning team and so will be involved in the development of e-MERLIN analysis strategies.

This project differs from the majority of the proposed legacy projects in having a sub-task focusing on spectral-line polarization. Between them, Vlemmings, Richards and Diamond have been responsible for the implementation of much of the interferometric spectropolarimetric data reduction software in use today and so understand the issues involved. Purcell and Hoare, working with Cotton of NRAO, have developed the calibration and, more importantly, the imaging pipeline for the VLA CORNISH survey. This was a major challenge since the pipeline had to produce accurate images in the presence of the complex, multi-scale background present in the Galactic Plane. So, the team has the appropriate skills and experience in place.

The project will have various work-packages (WPs), listed below along with the WP leaders and participants:

- WP1: observing schedules: Hoare,Vlemmings
- WP2: continuum calibration pipeline: Purcell
- WP3: spectral line calibration: Richards, Diamond
- WP4: continuum imaging pipeline: Purcell, Hoare
- WP5: spectral imaging calibration: Vlemmings, Richards, Diamond, Vlemmings, Fuller

Purcell and Richards will be responsible for monitoring the data quality. The continuum calibration pipeline used for this project will be the same as, or closely related to, the standard e-MERLIN pipeline. However, we will take on the role of developing the e-MERLIN spectral line polarization pipeline and will make it immediately available to the user community. As a contribution to the community we will provide a list of phase calibrators for the Galactic Plane using the recently reduced CORNISH survey results.

Science working groups: The science exploitation phase of this project will be organized around a series of Science Working Groups (SWGs), under which specific research projects, comparison with other existing surveys, follow-up observations with other instruments and at other wavebands will be undertaken by smaller groups and individuals with specific interests and skills. These SWGs will be set up in the 6-12 months after the formal allocation of time to the project. This timescale should be sufficient to allow leading members to bid for additional support for PhD students and PDRAs from STFC and other international funding bodies. Some resource has already been identified, e.g. Purcell (STFC funded PDRA at JBCA) and a PhD post at the University of Bonn, working with Vlemmings. The SWGs and their team leaders will be:

- IRDCs: Jackson
- Disc winds: Drew
- Jets: Torrelles
- Magnetic fields: Vlemmings
- Evolutionary sequence: Thompson
- Hyper-compact H II regions: Kurtz

The Need for Legacy Status

If this science was carried out under PATT driven PI programmes it will be done piecemeal and with little coordination. That will render any attempt to understand how the feedback processes vary systematically with age and mass hopelessly complicated due to the lack of any well-selected sample. Individual groups will propose for individual 'favorite objects' or small samples with widely varying criteria. That would seriously put back the attempts to understand massive star formation.

The data from this proposal will leave a great legacy for future models of massive star formation. In many ways the observations are ahead of the models at present with few simulations from first principles to test against, e.g. MHD jet models for massive forming stars. The tools to do these type of simulations are being put in place and should be available for testing around the end of the Legacy programme. In this context the magnetic field models constructed from the maser data will be an important input to the radiative transfer modeling tools that will be developed as part of the ARTIST collaboration (Adaptable Radiative Transfer Innnovations for Submm Telescopes; Univ. of Bonn, Leiden Univ. & CSIC-IEEC Barcelona), which aims provide the community with a convenient tool to model fully self-consistently the chemical and physical and polarization structure of objects observed at submillimeter wavelengths.

The clear well-defined selection criteria used here in terms of luminosity, colour and distance, will enable others to exploit the results for other purposes in the future, currently unforeseen. It is also clear that there will be other objects detected in the field of view around the targets that are of great interest. Most massive stars have associated clusters of lower mass stars and these often exhibit radio emission. The example of GGD27 in Figure 6 shows a cluster of radio objects around the MYSO. The emission from these objects is usually non-thermal, highly variable, gyro-synchrotron emission from the magnetically active T Tauri stars. e-MERLIN will detect many of these in the 3-7′ field of view that can be cross-matched and identified in deep near-IR and X-ray data to study the activity of the low-mass objects in clusters associated with massive stars. This will enable a systematic study of this behavior in clusters with a range of ages and central star mass.

Of course the scale of the Legacy programme is instrumental in bringing together a large international team that would not likely be so extensive if the science was carried out through smaller PI programmes. This proposal also brings together effort and input to the e-MERLIN commissioning which would not have happened otherwise.

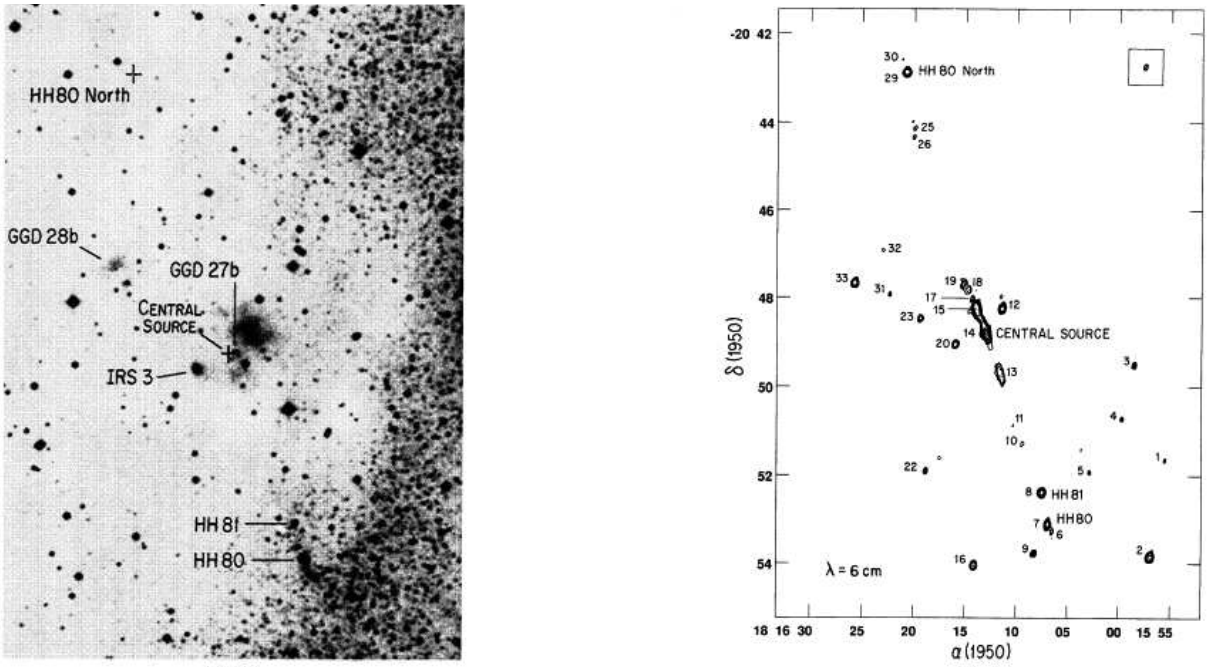

Figure 6: **(a)** Optical image of the HH80-81 region showing the shocked emission at the end of the radio jet. **(b)** Radio image of the jet showing a cluster of low-mass radio sources around it. From Marti et al. (1993).

Appendix A - Preliminary Target Lists

The target selection work is not yet complete, principally awaiting on the measurement of fluxes from the MIPSGAL survey. The tables below show the progress so far.

Table 1: Preliminary list of active IRDC targets - incomplete, awaiting MIPS flux measurements.

Name	RA			Dec		
18517+0437	18	54	13.80	+04	41	32.00
G019.27+00.07[a]	18	25	58.5	-12	03	59
G023.60+00.00	18	34	21.1	-08	18	07
G024.33+00.11[b]	18	35	07.7	-07	34	33
G024.33+00.11	18	35	07.9	-07	35	04
G024.60+00.08	18	35	35.7	-07	18	09
G027.97-00.42	18	43	58.0	-04	34	24
G028.37+00.07	18	42	50.7	-04	03	15
G028.37+00.07	18	43	12.9	-04	01	16
G031.97+00.07	18	49	33.0	-00	47	33
G033.69-00.01	18	52	58.1	-00	41	20
G034.43+00.24	18	53	18.0	-01	25	24
G33.64-0.21	18	53	28.70	+00	31	58.00
G33.68-0.26	18	53	45.20	+00	23	47.00
G35.02+0.35	18	54	00.60	+02	00	50.00
G41.34-0.14	19	07	21.87	+07	52	17.34
G43.80-0.13	19	11	55.10	+09	36	00.00
G49.57-0.38	19	23	53.60	+14	34	54.00
W48[c]	19	01	45.00	+01	13	33.00
W49N	19	10	13.52	+09	06	13.91
W51	19	23	43.90	+14	30	31.00
G108.18+5.51	22	28	52.00	+64	13	22.00

a) Note: This and the following 10 sources are selected as 24μm sources in IRDCs. The others are methanol maser sources known not to be mid-IR bright but still awaiting confirmation as genuine IRDC sources.
b) Note: This and the following source will be covered by a single pointing
b) Note: These names do not refer to the main H II region but these sources are in the vicinity.

Table 2: Preliminary list of MYSOs - almost complete, awaiting final kinematic distance determinations in RMS survey.

Name	RA			Dec		
G017.6380+00.1566	18	22	26.33	-13	30	12.2
G023.3891+00.1851	18	33	14.40	-08	23	57.5
G023.6566-00.1273	18	34	51.60	-08	18	21.6
G025.4118+00.1052	18	37	16.99	-06	38	25.4
G027.7954-00.2772	18	43	2.35	-04	41	48.8
G030.1981-00.1691	18	47	3.10	-02	30	36.0
G030.8185+00.2729	18	46	36.62	-01	45	22.3
G034.7123-00.5946	18	56	48.24	+01	18	47.5
G035.1979-00.7427	18	58	13.08	+01	40	39.4
G039.4943-00.9933	19	6	59.79	+05	22	54.8
G050.7796+00.1520	19	24	17.48	+15	54	4.7
G052.9217+00.4142	19	27	34.89	+17	54	38.5
G075.7666+00.3424	20	21	41.47	+37	25	51.2
G076.3829-00.6210	20	27	26.67	+37	22	47.6
G077.4052-01.2136	20	32	54.05	+37	51	29.2
G077.8999+01.7678	20	21	54.89	+39	59	45.2
G078.1224+03.6320	20	14	26.30	+41	13	31.4
G078.8867+00.7087	20	29	24.91	+40	11	19.3
G081.8652+00.7800	20	38	35.9	+42	37	22
G094.3228-00.1671	21	31	45.17	+51	15	35.6
G094.4637-00.8043	21	35	9.51	+50	53	10.0
G094.6028-01.7966	21	39	58.54	+50	14	20.4
G100.3779-03.5784	22	16	10.42	+52	21	33.8
S140 IRS1	22	19	18.4	+63	18	45
G102.8051-00.7184	22	19	9.21	+56	5	2.0
G108.2118-01.2887	22	55	59.66	+58	14	40.9
G108.4714-02.8176	23	2	32.04	+56	57	53.3
G109.8715+02.1156	22	56	17.97	+62	1	54.5
G110.0931-00.0641	23	5	25.08	+60	8	16.1
G111.5423+00.7776	23	13	45.34	+61	28	13.1
G114.0835+02.8568	23	28	27.86	+64	17	37.3
G126.7144-00.8220	1	23	32.93	+61	48	49.0
G134.2792+00.8561	2	29	1.97	+61	33	31.7
G138.2957+01.5552	3	1	31.63	+60	29	12.1
G141.9996+01.8202	3	27	38.62	+58	47	1.3
G142.2446+01.4299	3	27	31.22	+58	19	23.2
G143.8118-01.5699	3	24	51.05	+54	57	30.6
G148.1201+00.2928	3	56	15.12	+53	52	12.4
G174.1974-00.0763	5	30	46.08	+33	47	53.2
Mon R2 IRS3	06	07	47.8	-06	22	55
G188.9479+00.8871	6	8	53.83	+21	38	25.4
G192.6005-00.0479	6	12	54.05	+17	59	22.6
G194.9349-01.2224	6	13	16.13	+15	22	40.8
G196.4542-01.6777	6	14	36.98	+13	49	34.7
G203.3166+02.0564	6	41	10.13	+09	29	33.7

Table 3: Preliminary list of candidate HCHIIs - almost complete, awaiting completion of CORNISH data processing.

Name	RA			Dec		
G018.8246-00.4673	18	26	59.02	-12	44	47.0
G025.7161+00.0486	18	38	2.88	-06	23	46.0
G027.1852-00.0812	18	41	13.15	-05	8	59.6
G028.2007-00.0494	18	42	58.18	-04	13	56.3
G032.9275+00.6063	18	49	16.32	+00	16	21.7
G042.1099-00.4466	19	9	53.61	+07	57	18.4
G043.3061-00.2106	19	11	16.94	+09	7	30.0
G045.0711+00.1325	19	13	22.01	+10	50	53.5
G045.4658+00.0457	19	14	25.61	+11	9	27.0
G048.9289-00.2795	19	22	14.81	+14	3	58.3
G048.9289-00.2795	19	22	14.81	+14	3	58.3
G048.9897-00.2992	19	22	26.21	+14	6	37.8
G048.9897-00.2992	19	22	26.21	+14	6	37.8
G053.9584+00.0317	19	31	5.26	+18	38	15.4
G069.5395-00.9754	20	10	8.98	+31	31	34.3
G070.3329+01.5864	20	1	55.22	+33	34	19.9
G077.4622+01.7600	20	20	39.21	+39	37	53.0
G079.1272+02.2782	20	23	23.88	+41	17	39.1
G079.3202+01.3131	20	28	10.20	+40	53	38.0
G080.8645+00.4197	20	36	52.27	+41	36	23.8
G083.7962+03.3058	20	33	48.12	+45	40	53.8
G085.4102+00.0032	20	54	13.75	+44	54	6.8
G098.0361+01.4462	21	43	1.46	+54	56	19.0
G109.0974-00.3458	22	59	6.12	+59	28	27.5
G125.6045+02.1038	1	16	36.72	+64	50	41.3
G133.7150+01.2155	2	25	40.73	+62	5	52.8
G133.9476+01.0648	2	27	4.06	+61	52	26.0
G139.9091+00.1969	3	7	23.95	+58	30	49.3
G155.3319+02.5989	4	40	27.22	+50	28	29.3
G173.4815+02.4459	5	39	12.96	+35	45	51.5
G207.2654-01.8080	6	34	37.70	+04	12	42.8